

Breaking the Rate-Loss Bound of Quantum Key Distribution with Asynchronous Two-Photon Interference

Yuan-Mei Xie,^{1,*} Yu-Shuo Lu,^{1,*} Chen-Xun Weng,¹ Xiao-Yu Cao,¹ Zhao-Ying Jia,¹ Yu Bao,¹ Yang Wang,¹ Yao Fu,² Hua-Lei Yin,^{1,†} and Zeng-Bing Chen^{1,2,‡}

¹*National Laboratory of Solid State Microstructures,
School of Physics and Collaborative Innovation Center of Advanced
Microstructures, Nanjing University, Nanjing 210093, China.*
²*MatricTime Digital Technology Co. Ltd., Nanjing 211899, China*

Twin-field quantum key distribution can overcome the secret key capacity of repeaterless quantum key distribution via single-photon interference. However, to compensate for the channel fluctuations and lock the laser fluctuations, the techniques of phase tracking and phase locking are indispensable in experiment, which drastically increase experimental complexity and hinder free-space realization. We herein present an asynchronous measurement-device-independent quantum key distribution protocol that can surpass the secret key capacity even without phase tracking and phase locking. Leveraging the concept of time multiplexing, asynchronous two-photon Bell-state measurement is realized by postmatching two interference detection events. For a 1 GHz system, the new protocol reaches a transmission distance of 450 km without phase tracking. After further removing phase locking, our protocol is still capable of breaking the capacity at 270 km. Intriguingly, when using the same experimental techniques, our protocol has a higher key rate than the phase-matching-type twin-field protocol. In the presence of imperfect intensity modulation, it also has a significant advantage in terms of the transmission distance over the sending-or-not-sending type twin-field protocol. With high key rates and accessible technology, our work provides a promising candidate for practical scalable quantum communication networks.

I. INTRODUCTION

Quantum key distribution (QKD) [1, 2] allows the distribution of information-theoretically secure keys guaranteed by quantum mechanical limits. However, experimental implementations of QKD always deviate from the theoretical assumptions used in security proofs, leading to various quantum hacking attacks [3–7]. Fortunately, all security loopholes on the detection side are closed by measurement-device-independent QKD (MDIQKD) [8], which introduces an untrusted third party, Charlie, to perform two-photon Bell-state measurement in the intermediate node. Thus far, MDIQKD has made many theoretical and experimental breakthroughs [9–25].

However, because a significant number of photons are inevitably lost in the channel, the key rate of most QKD protocols, including MDIQKD, is rigorously limited by the secret key capacity of repeaterless QKD [26–30], more precisely, the Pirandola–Laurenza–Ottaviani–Banchi (PLOB) bound $R = -\log_2(1 - \eta)$ [28], where R is the secret key rate and η is the total channel transmittance between the two users. Utilizing single-photon interference, twin-field QKD (TFQKD) [31] and its variants [32–43], such as sending-or-not-sending QKD (SNSQKD) [33] and phase-matching QKD (PMQKD) [32, 40], have been proposed to increase the key rate to $O(\sqrt{\eta})$, overcoming the PLOB

bound. Since then, they have aroused widespread concern. For example, remarkable progress has been made in the theory of finite key analysis [44–47]. Additionally, some notable experimental implementations have been reported [48–60]. The longest transmission distance of more than 830 km was recently achieved in the laboratory through optical fibers [60].

Because the phase evolution of the twin fields is sensitive to both channel length drift and frequency difference between two user lasers, phase-tracking and phase-locking techniques are vital for twin-field-type protocols. Phase tracking is used to compensate for the phase fluctuation on the channels connecting the users to Charlie, where bright reference light pulses are sent to measure the phase fluctuation. However, the performance of the system is severely affected because the bright light causes scattering noise and occupies the time of the quantum signal [48, 50–54, 56]. Phase tracking also imposes a high counting requirement on the detectors. Phase locking is utilized to lock the frequency and the phase of the two users' lasers. There are several types of phase-locking techniques, including laser injection [17], optical phase-locked loop [61, 62], and time-frequency dissemination technology [51, 63]. However, they all require additional channels between users to transfer the reference light. In addition, laser injection may introduce security risks [64, 65], and the optical phase-locked loop and the time-frequency dissemination technology both require complicated feedback systems. An ingenious replacement for phase locking and phase tracking in TFQKD experiments [49, 55] is the plug-and-play type construction [34], but it is susceptible to Trojan horse attacks [66–69]. Furthermore, free-space realization of

* These authors contributed equally to this work

† hlyin@nju.edu.cn

‡ zbchen@nju.edu.cn

QKD in various types of channels, including the atmosphere [70, 71], seawater [72], and satellite-to-ground channels [73–76], is essential to establishing a global-scale quantum networks [77, 78]. However, deploying phase-tracking and phase-locking techniques in free space faces some technical challenges. For example, phase locking requires additional channels between the two users. In summary, these technical requirements increase experimental complexity, may incur security risks, and hinder the implementation of TFQKD in commerce and free space.

In this work, we propose an asynchronous-MDIQKD protocol to remove these requirements. It has a simple hardware implementation while enjoying a high key rate. Recall that in the conventional time-bin encoding MDIQKD scheme [79], coincidence detection of two neighboring time bins is required, resulting in the $O(\eta)$ scaling of the key rate [30]. Intriguingly, we observe that the two neighboring time bins can actually be decoupled. Specifically, the requirement for coincidence detection of two neighboring time bins is unnecessary. By utilizing time multiplexing, we match two detected time bins that are phase-correlated to establish an asynchronous two-photon Bell state, and the key rate is enhanced to $O(\sqrt{\eta})$. This can be regarded as breaking the recently proposed linear boundary of dual-rail protocols [30]. We highlight the intrinsic differences between time-bin encoding MDIQKD and polarization encoding MDIQKD—time multiplexing is possible solely for time-bin encoding, where there are infinite time modes. For polarization encoding, only two orthogonal modes exist.

Because the differential phase evolution of each time bin is approximately equal in a short time interval, we can postmatch two phase-related time bins without the phase-tracking and phase-locking techniques at the cost of a slight increase in the interference error rate. We show that after removing these techniques, the misalignment angle between the two users is approximately 0.1π within $1\ \mu\text{s}$ with simple commercially available instruments, giving rise to an interference error rate of approximately 2.4%. In this case, our protocol can beat the PLOB bound at a distance of approximately 270 km, achieving a reasonable trade-off between practicality and performance. By circumventing the need for phase locking and phase tracking, our protocol can directly utilize techniques derived from free-space MDIQKD [70], thereby facilitating QKD to break the secret key capacity in free space. Moreover, when the imperfection in light intensity modulation is considered [80], our protocol achieves a longer transmission distance and higher key rates compared with SNSQKD with actively odd-parity pairing (AOPP) [81, 82] and PMQKD [40] when using the same experimental techniques.

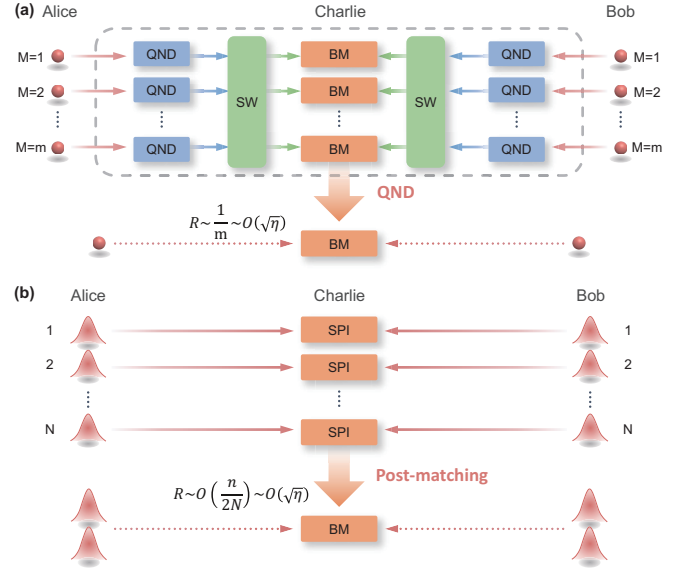


FIG. 1. Basic idea of the adaptive MDIQKD scheme [83] and this work. (a) In the adaptive MDIQKD scheme, Alice and Bob send m single-photon pulses to Charlie using spatial multiplexing. Charlie applies quantum nondemolition measurement (QND) to confirm the arrival of pulses, matches the arriving pulses using optical switches (SW), and performs two-photon Bell measurements (BM) on the pairs. (b) In our asynchronous-MDIQKD protocol, Alice and Bob send N pulses to Charlie to perform single-photon interference (SPI), and a two-photon Bell state is obtained by postmatching two successful SPI events.

II. ASYNCHRONOUS-MDIQKD PROTOCOL

In this section, we first introduce the basic idea of the asynchronous-MDIQKD protocol and then present a detailed protocol description.

A. Protocol topology

Our proposal is motivated by the adaptive MDIQKD scheme [83], as shown in Fig. 1(a). In this scheme, the idea of spatial multiplexing is leveraged, where m optical pulses in single-photon states pass through m channels. When $m\sqrt{\eta} \geq 1$, one or more single photons arrive at Charlie from Alice and Bob each, with unitary probability, resulting in $O(\sqrt{\eta})$ scaling with the key rate.

In the time-bin encoding MDIQKD [79], the information is encoded in the relative phase between the optical modes in two separate time bins i, j , with $i = 2t - 1$, $j = 2t$, where t is an integer. Let $|1, 0\rangle^{i,j} = |1\rangle^i |0\rangle^j$ denote the quantum state, where there is one photon in time bin i and zero photon in time bin j . Alice and Bob prepare quantum states $|+z\rangle = |1, 0\rangle^{i,j}$, $|-z\rangle = |0, 1\rangle^{i,j}$, and $|\pm x\rangle = (|1, 0\rangle^{i,j} \pm |0, 1\rangle^{i,j})/\sqrt{2}$, and send them to Charlie for Bell-state measurement, where $|\pm z\rangle$ are the eigenstates in the Z basis, and $|\pm x\rangle$ are the eigenstates in

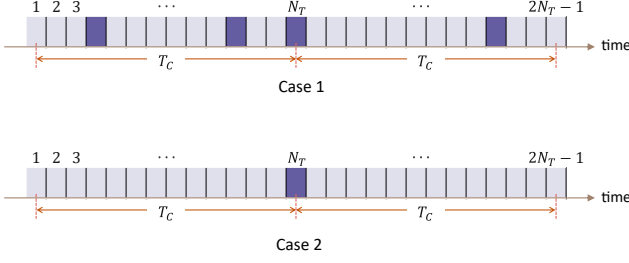


FIG. 2. Schematic of *case 1* and *case 2*. Each time bin is represented by a lattice, and detection events are painted in deep purple. *case 1*: a detection event around which other detection events can be found within T_c ; *case 2*: a detection event around which there are no other detection events within T_c . N_T is the total number of pulses sent within T_c , which is proportional to the system repetition rate.

the X basis. Note that for the Bell states announced by Charlie, $|\psi^\pm\rangle = 1/\sqrt{2}(|1,0\rangle_a^{i,j}|0,1\rangle_b^{i,j} \pm |0,1\rangle_a^{i,j}|1,0\rangle_b^{i,j})$, where subscript a represents mode “Alice” and b represents mode “Bob”, we can decouple i and j as two independent variables [84], making time multiplexing possible.

The basic idea of our asynchronous-MDIQKD protocol is illustrated in Fig. 1(b). N pairs of optical pulses are sent in N time bins. In each time bin, single-photon interference is performed, and $n \approx N\sqrt{\eta}$ successful detection events are obtained. By time multiplexing, Alice and Bob can postmatch successful detection events of two time bins that are phase-correlated to establish two-photon entangled states $|\psi^\pm\rangle$, leading to the $O(\sqrt{\eta})$ decay of the key rate.

We consider the case in which Alice and Bob always match two successful detection events within a short time interval T_c , where T_c is on the order of microseconds. Hereafter, we abbreviate a successful detection event to a detection event for simplicity. As shown in Fig. 2, the detection events can be classified into two cases: *case 1* and *case 2*. The *case 1* event indicates that other detection events can be found around it within T_c , and the differential phase evolution of detection events in T_c are unknown but almost the same. The *case 2* event indicates that there are no other detection events around it within T_c . After removing phase tracking and phase locking, the differential phase evolution of each *case 2* event becomes indeterminate. This means that *case 2* events have no phase correlations with each other. These events should be carefully handled to ensure security. For example, Charlie can know the total photon number in each optical pulse pair sent by Alice and Bob via quantum nondemolition measurements, and Charlie always lets the joint single-photon be detected as *case 2* events. Charlie’s operation would not be found by Alice and Bob. If Alice and Bob discard *case 2* events, the single-photon pairs cannot be reasonably estimated using the conventional decoy-state method. Fortunately, a suf-

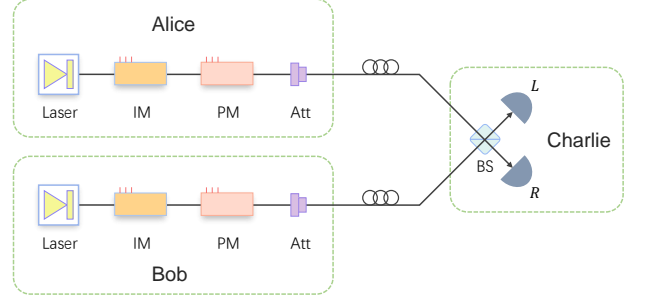


FIG. 3. Schematic of the setup for the asynchronous-MDIQKD protocol. Alice and Bob utilize a narrow-linewidth continuous-wave laser, intensity modulator (IM), phase modulator (PM), and attenuator (ATT) to prepare phase-randomized weak coherent pulses with different intensities and phases. Charlie performs interference measurement with a beam splitter (BS) and single-photon detectors. Charlie announces the detection events where only the detector **L** or **R** clicks.

ficiently small number (one on average) of *case 2* events will not affect the security of the protocol.

B. Protocol description

The schematic of the asynchronous-MDIQKD setup is shown in Fig. 3, and the details of the protocol are presented as follows.

1. Preparation. Alice and Bob repeat the first two steps for N rounds to obtain sufficient data. At each time bin $i \in \{1, 2, \dots, N\}$, both phase $\theta_a^i \in [0, 2\pi)$ and classical bit $r_a^i \in \{0, 1\}$ are randomly chosen by Alice. Alice then prepares a weak coherent pulse $|e^{i(\theta_a^i + r_a^i \pi)} \sqrt{k_a^i}\rangle$ with probability p_{k_a} , where $k_a^i \in \{\mu_a, \nu_a, \mathbf{o}_a, \hat{\mathbf{o}}_a\}$ corresponds to the signal, decoy, preserve-vacuum, and declare-vacuum intensities, respectively ($\mu_a > \nu_a > \mathbf{o}_a = \hat{\mathbf{o}}_a = 0$). Similarly, Bob prepares a phase-randomized weak coherent pulse. Alice and Bob send the corresponding pulses $|e^{i(\theta_a^i + r_a^i \pi)} \sqrt{k_a^i}\rangle$ and $|e^{i(\theta_b^i + r_b^i \pi)} \sqrt{k_b^i}\rangle$ ($k_b^i \in \{\mu_b, \nu_b, \mathbf{o}_b, \hat{\mathbf{o}}_b\}$) to Charlie via insecure quantum channels.

2. Measurement. For each time bin i , Charlie performs interference measurement on the two received pulses. Charlie obtains a detection event when only one detector clicks. He publicly announces whether a detection event is obtained and which detector clicked. In the following description, we define $\{k_a, k_b\}$ as a detection event when Alice sends intensity k_a , and Bob sends k_b . The compressed notation $\{k_a^i k_b^j\}$ indicates that $\{k_a^i, k_b^j\}$ and $\{k_b^j, k_a^i\}$ are matched, the first label referring to time bin i , and the second to time bin j .

3. Sifting. Alice and Bob first check the number of *case 2* events. If the number of occurrences of *case 2* is smaller than or equal to Λ , the data of *case 2* can be discarded, where Λ is a preset threshold; otherwise,

they abort the protocol. For *case 1* events, when at least either Alice or Bob chooses a decoy or declare-vacuum intensity, they announce their intensities and phase information through authenticated channels. They then use the following rules to randomly match two *case 1* events with a time interval of less than T_c .

The unannounced detection events $\{\mu_a, \mathbf{o}_b\}$, $\{\mu_a, \mu_b\}$, $\{\mathbf{o}_a, \mu_b\}$, and $\{\mathbf{o}_a, \mathbf{o}_b\}$ are used to form data in the Z basis. For these events, Alice randomly matches a time bin i of intensity μ_a with another time bin j of intensity \mathbf{o}_a . Alice and Bob discard detection events that cannot find a matchable peer. Then, Alice sets her bit value to 0 (1) if $i < j$ ($i > j$) and informs Bob of the serial numbers i and j . In the corresponding time bins, if Bob chooses intensities $k_b^{\min\{i,j\}} = \mu_b$ (\mathbf{o}_b) and $k_b^{\max\{i,j\}} = \mathbf{o}_b$ (μ_b), the bit value is set to 0 (1). Bob announces an event where $k_b^i = k_b^j = \mathbf{o}_b$ or μ_b . Thus, the valid events in the Z basis are $\{\mu_a \mathbf{o}_a, \mathbf{o}_b \mu_b\}$, $\{\mu_a \mathbf{o}_a, \mu_b \mathbf{o}_b\}$, $\{\mathbf{o}_a \mu_a, \mathbf{o}_b \mu_b\}$, and $\{\mathbf{o}_a \mu_a, \mu_b \mathbf{o}_b\}$.

The detection events $\{\nu_a, \nu_b\}$, $\{o_a, \nu_b\}$, $\{\nu_a, o_b\}$, $\{\hat{o}_a, o_b\}$, and $\{\mathbf{o}_a, \hat{o}_b\}$ are used to form data in the X basis, where $o_{a(b)} \in \{\mathbf{o}_{a(b)}, \hat{o}_{a(b)}\}$. The global phase of Alice (Bob) at time bin i is defined as $\varphi_{a(b)}^i := \theta_{a(b)}^i + \phi_{a(b)}^i$, where $\phi_{a(b)}^i$ is the phase evolution from the channel. The global phase difference between Alice and Bob at time bin i is $\varphi^i = \varphi_a^i - \varphi_b^i$. Alice and Bob randomly choose two detection events that satisfy $k_a^i = k_a^j$, $k_b^i = k_b^j$ and $|\varphi^i - \varphi^j| = 0$ or π (experimental techniques for quantifying $|\varphi^i - \varphi^j|$ are discussed later in Sec. III). They then match the two events as $\{k_a^i k_a^j, k_b^i k_b^j\}$. By calculating the classical bits $r_a^i \oplus r_a^j$ and $r_b^i \oplus r_b^j$, Alice and Bob obtain a bit value in the X basis, respectively. Afterwards, in the Z basis, Bob always flips his bit. In the X basis, Bob flips part of his bits to correctly correlate them with Alice's (see Table. I).

4. *Parameter estimation.* Alice and Bob exploit the random bits from the Z basis to form the n^z -length raw key bit. The remaining bits in the Z basis are used to calculate the bit error rate E^z . They reveal all bit values in the X basis to obtain the total number of errors. The decoy-state method [85, 86] is utilized to estimate the number of vacuum events in the Z basis $s_{0\mu_b}^z$, number of single-photon pairs s_{11}^z , bit error rate in the X basis e_{11}^x , and phase error rate of single-photon pairs ϕ_{11}^z in the Z basis (see Appendix A for details).

Note: To estimate the single-photon component gain of each postmatching interval, we assume that the single-photon distributions in all detection events are independent and identical.

5. *Postprocessing.* Alice and Bob distill the final keys by using the error correction algorithm with ε_{cor} -correct, and the privacy amplification algorithm with ε_{sec} -secret. Similar to Ref. [15], the length of the final secret key ℓ

with total security $\varepsilon_{\text{AMDI}} = \varepsilon_{\text{sec}} + \varepsilon_{\text{cor}}$ can be given by

$$\ell = s_{0\mu_b}^z + s_{11}^z \left[1 - H_2(\bar{\phi}_{11}^z) \right] - \lambda_{\text{EC}} - \log_2 \frac{2}{\varepsilon_{\text{cor}}} - 2 \log_2 \frac{2}{\varepsilon' \hat{\varepsilon}} - 2 \log_2 \frac{1}{2\varepsilon_{\text{PA}}}, \quad (1)$$

where \underline{x} and \bar{x} denote the lower and upper bounds of the observed value x , respectively. $\lambda_{\text{EC}} = n^z f H_2(E^z)$ is the amount of information leaked during error correction, where f is the error correction efficiency, and $H_2(x) = -x \log_2 x - (1-x) \log_2 (1-x)$ is the binary Shannon entropy function. ε_{cor} is the failure probability of error verification, and ε_{PA} refers to the failure probability of privacy amplification. ε' and $\hat{\varepsilon}$ represent the coefficients when using the chain rules of smooth min-entropy and max-entropy, respectively. $\varepsilon_{\text{sec}} = 2(\varepsilon' + \hat{\varepsilon} + 2\varepsilon_e) + \varepsilon_\beta + \varepsilon_0 + \varepsilon_1 + \varepsilon_{\text{PA}}$, where ε_0 , ε_1 and ε_e are the failure probabilities of estimating the terms $s_{0\mu_b}^z$, s_{11}^z , and ϕ_{11}^z , respectively.

III. EXPERIMENTAL DISCUSSION

In the asynchronous-MDIQKD protocol, the information in the interference mode is encoded in the phase difference of two matched time bins. One may regard the latter as the reference mode and the former as the signal mode, which is the same as the time-bin encoding MDIQKD [79]. In the X basis, Alice and Bob post-match pulses of two time bins i and j with phase relation $|\varphi^i - \varphi^j| = 0$ or π , where $\varphi^{i(j)} = \theta_a^{i(j)} - \theta_b^{i(j)} + \phi^{i(j)}$ is the global phase difference at time bin i (j). $\theta_a^{i(j)}$ and $\theta_b^{i(j)}$ are random phases known to Alice and Bob. $\phi^{i(j)} = \phi_a^{i(j)} - \phi_b^{i(j)}$ is the differential phase evolution at time bin i (j), which is determined by the frequency difference between the two users' lasers and the fluctuation of the fiber channels. When the two pulses sent by Alice and Bob reach Charlie, the phase evolutions of the two pulses are $\phi_a^i = 2\pi v_a^i(t^i - l_a^i/s)$ and $\phi_b^i = 2\pi v_b^i(t^i - l_b^i/s)$, respectively, where t^i is the time of the time bin i , $v_{a(b)}^i$ is the laser frequency, s is the speed of light in the fiber, and $l_{a(b)}^i$ is the fiber length between Alice (Bob) and Charlie at time bin i . In symmetric channels, the differential

TABLE I. Postprocessing of bit in the sifting step. In the X basis, Bob decides whether to implement a bit flip to guarantee correct correlations, depending on the clicking detectors announced by Charles and the global phase difference between two matching time bins. Here, **RL** (**LR**) denotes the detectors **R** (**L**) and **L** (**R**) clicks at time bins i and j , respectively. **RR** (**LL**) denotes that the detector **R** (**L**) clicks at time bins i and j .

Measurement results of Charlie		
Global phase difference	RL (LR)	RR (LL)
$ \varphi^i - \varphi^j = 0$	Bit flip	No bit flip
$ \varphi^i - \varphi^j = \pi$	No bit flip	Bit flip

phase evolution between Alice and Bob can be expressed as

$$\phi^i = \phi_a^i - \phi_b^i = 2\pi\delta v^i t^i - \frac{2\pi}{s}(\delta v^i l^i + v^i \delta l^i), \quad (2)$$

where $\delta v^i = v_a^i - v_b^i$, $\delta l^i = l_a^i - l_b^i$, $l^i = (l_a^i + l_b^i)/2$ and $v^i = (v_a^i + v_b^i)/2$. Ensuring the phase correlation between time bins i and j is essential for postmatching. In the experiment, when the time interval for postmatching T_c is large, the phase correlation can be maintained by using phase-tracking and phase-locking techniques to measure differential phase evolution in each time bin. Fortunately, when T_c is small, the phase correlation naturally exists, that is, the differential phase evolution is approximately constant within T_c because the fiber length drift rate and relative phase drift rate between lasers are relatively small. Therefore, our protocol can discard phase-tracking and phase-locking techniques at the cost of a slight increase in the interference error rate.

A. Removing phase tracking

Assuming that the frequencies of the two user lasers are synchronized with phase-locking techniques, $v_a^{i(j)} = v_b^{i(j)} = v^{i(j)}$, we have

$$\phi^j - \phi^i = \frac{2\pi}{s} (v^j \delta l^j - v^i \delta l^i). \quad (3)$$

When T_c is on the order of tens of microseconds, say $50 \mu s$, the frequency drift is small for typical commercially available narrow-linewidth lasers. Hence, $\phi^j - \phi^i$ is mainly determined by the relative phase drift caused by the fiber length drift, which was measured to be approximately $8 \text{ rad/ms} @ 402 \text{ km}$ [52], corresponding to a phase drift of 0.4 rad per $50 \mu s$. Note that two time bins i and j are randomly and uniformly distributed within the time interval T_c ; therefore, the mean phase drift between the two time bins is half of the maximum value. Consequently, there will be an intrinsic interference error rate of approximately $(1 - \cos 0.2)/2 \approx 1\%$.

This indicates that our protocol with short-term matching can be experimentally implemented without phase tracking when the matching interval T_c is on the order of tens of microseconds. Note that sufficient detection counts should be accumulated per T_c for postmatching. The detection count per T_c can be approximated as $T_c F(1 - e^{-\bar{\mu}\eta_d\sqrt{\eta_{ch}}})$, where F is the system frequency, η_{ch} is the channel transmittance between Alice and Bob, η_d is the detection efficiency, and $\bar{\mu}$ is the total mean photon number of Alice and Bob. At 400 km , by using a 1 GHz system with $\eta_d = 70\%$ and ultra-low loss fiber, there will be approximately 9.3 detection events per T_c if we set $\bar{\mu} = 0.5$, which is sufficient for postmatching.

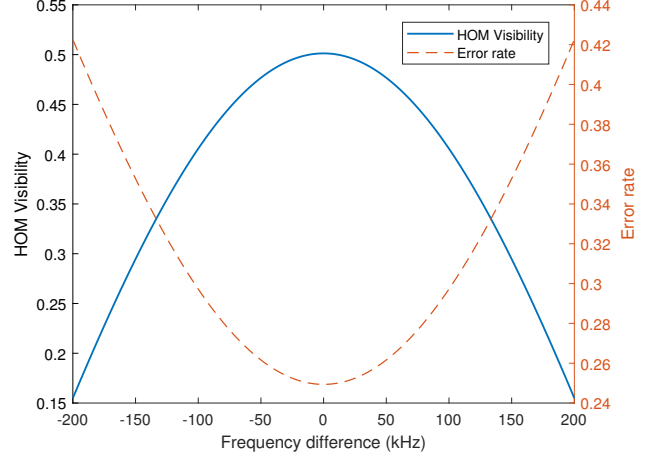


FIG. 4. HOM visibility and error rate as a function of frequency difference between two lasers δv . We set the time interval of two consecutive time bins $\tau = 1 \mu s$. The blue line is the HOM visibility, and the orange dotted line is the interference error rate.

B. Removing phase tracking and phase locking

We consider the case in which neither phase-tracking nor phase-locking techniques are applied. When T_c is on the order of a few tens of microseconds, the fiber length drift is also negligible. The relative phase drift between time bins i and j is mainly determined by the frequency difference between the two independent lasers, which can be expressed as

$$\phi^j - \phi^i = 2\pi\delta v(t^j - t^i). \quad (4)$$

In practice, δv is the sum of stable laser frequency difference between the two users and laser frequency random drift. The former can be a relatively large value (up to tens of megahertz) known to Alice and Bob. The latter is an unknown small value (tens of kilohertz). For simplicity, below we discuss the case where the two users try to adjust their lasers to nearly the same frequency, leaving only an unknown small δv . In this case, there is an intrinsic phase misalignment $\pi\delta v T_c$ on average during T_c . If δv is controlled to 100 kHz , for $T_c = 1 \mu s$, $\phi^i - \phi^j \approx 0.1\pi$, resulting in an interference error rate of 2.4% . By using an experimental setup with $F = 10 \text{ GHz}$ (which is feasible under current technology [87, 88]) and $\eta_d = 70\%$, at 300 km , there will be approximately 11.7 detection events per microsecond if we set $\bar{\mu} = 0.5$.

The experimental requirement of the asynchronous-MDIQKD protocol without phase tracking and phase locking is similar to that of the previous phase encoding MDIQKD, in which the information is encoded in the relative phase of the two time bins with time interval τ . The frequency difference between the two users will inevitably misalign the phase basis, leading to intrinsic phase misalignment $\delta\phi = 2\pi\delta v\tau$ [22]. In experimental

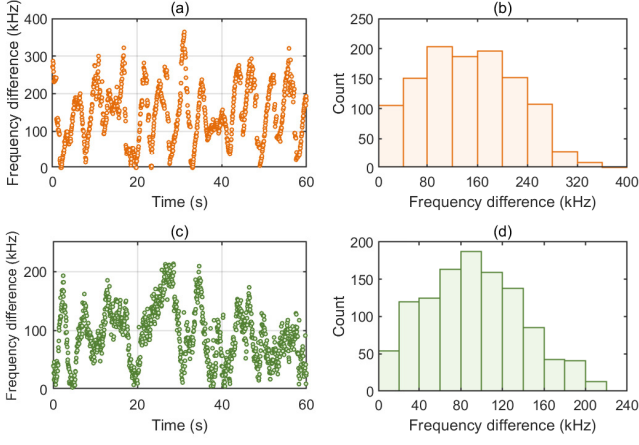


FIG. 5. Test results of the frequency difference between two independent lasers, which are obtained by manually adjusting the temperature. (a) Frequency difference between two NKT lasers for 60 s. (b) Histogram of the frequency difference distribution between the two NKT lasers. The mean frequency difference is 145 kHz. (c) Frequency difference between two RIO Orion lasers of 60 s. (d) Histogram of the frequency difference distribution between two RIO Orion lasers, where the mean value is 92.5 kHz. Note that if using automatic feedback systems, the frequency difference can be further reduced.

demonstrations in Refs. [18] and [22], the time delays are 6.37 ns and 0.5 ns, respectively. The maximum frequency difference is 37.5 MHz and 30 MHz, respectively, which introduce phase misalignments of 0.47π and 0.03π , respectively. For our protocol with short time matching, τ is on the order of microseconds, and the frequency difference is approximately tens of kilohertz.

In a real setup, to suppress the frequency difference between two independent lasers within 100 kHz, Alice and Bob can periodically enter the calibration process to calibrate the frequency of their lasers. There are several approaches available for frequency calibration. The most straightforward way is to measure the beat note of two lasers. Alice and Bob can also locally calibrate the frequency with a frequency standard [70]. In addition, they can measure the Hong-Ou-Mandel (HOM) interference and utilize the interference visibility as the feedback signal [25] to minimize the frequency difference. These are mature techniques in time-bin MDIQKD.

We briefly describe the method of frequency calibration using HOM interference [25] as follows. Consider the HOM interference of two weak coherent pulses with the same time, polarization and spatial mode, but different frequencies. The HOM interference visibility is related to the time interval of two consecutive time bins τ and the frequency difference δv . As shown in Fig. 4, we simulate the interference visibility V and interference error rate $E = (1 - V)/2$ as a function of δv , where $\tau = 1\ \mu\text{s}$. The visibility reaches the maximum value of approximately 0.5 when the frequency difference is 0, and decreases rapidly as the frequency difference increases.

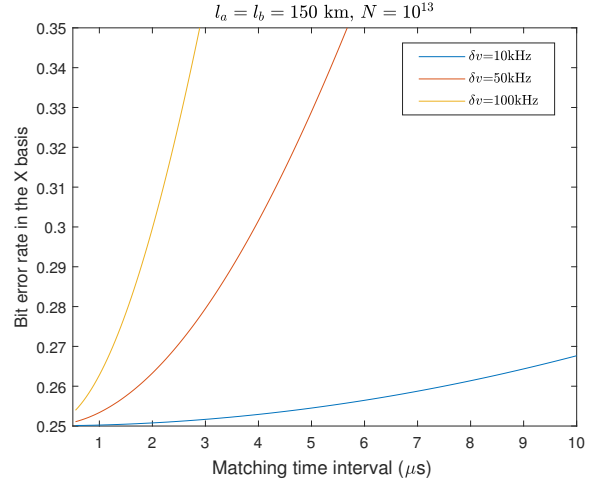


FIG. 6. The bit error rate in the X basis as a function of the matching time interval T_c , where both phase tracking and phase locking are not adopted. The distance between Alice and Bob is 300 km and the system repetition rate is $F = 4$ GHz. The frequency difference δv is set to 10, 50 and 100 kHz.

The minimum error rate of approximately 25% is obtained when $\delta v = 0$. When δv increases to 100 kHz, the error rate increases to 29.7%. In experiment, one can adjust the laser frequency to minimize the error rate. When the observed error rate is close to 25%, the frequencies of the two users' lasers are calibrated. By increasing τ , the error rate becomes more sensitive to δv .

To demonstrate the feasibility of the experimental setup without phase-tracking and phase-locking techniques, we measured the frequency difference between two independent lasers. Two narrow-linewidth lasers working at 1550.12 nm emit continuous light. The continuous light passes through fiber, interferes at a beam splitter, and is detected by a photoelectric detector. The beat note was recorded using an oscilloscope. Fig. 5 (a) shows the beat frequencies of the two NKT lasers (Koheras BASIK E15). These lasers support fine piezoelectric tuning with a minimum tuning frequency on the order of kHz. During the test time of 60 s, we manually adjusted the frequency of one of the lasers every few seconds to minimize the observed beat frequency. A histogram of the recorded data is presented in Fig. 5(b), and the mean value is 145 kHz. We also measured the frequency difference between the two independent Rio lasers (Rio ORION). They were first tuned to the same frequency and kept free running during the 60 s test time. The collected data are shown in Fig. 5(c), and the histogram is shown in Fig. 5(d), with an average of 92.5 kHz. In a real setup, if using the RIO laser or the NKT laser, the frequency needs to be adjusted every few seconds. We stress that the frequency difference can be further reduced by utilizing automatic feedback systems and improving the stability of the experimental environment.

Additionally, we simulate the bit error rate in the X

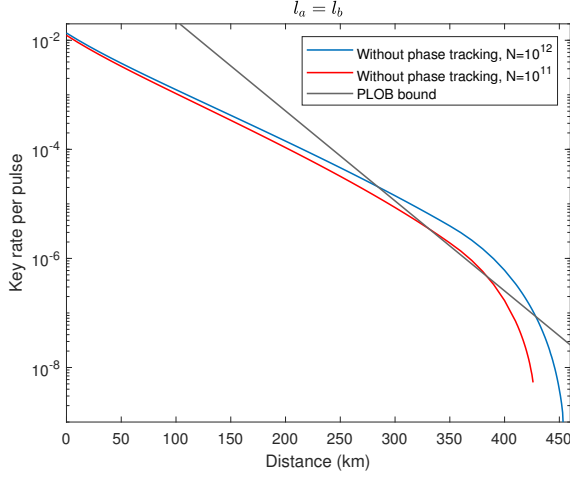


FIG. 7. Secret key rates of the asynchronous-MDIQKD with short time matching as a function of the distance when implemented without phase tracking. Here, we set the matching time interval $T_c = 50 \mu\text{s}$, the system repetition rate is $F = 1 \text{ GHz}$ and the angle of misalignment in the X basis $\sigma = \pi/10$. Our protocol can break the PLOB bound at a distance of approximately 280 km with $N = 10^{12}$, and the transmission distance reaches 450 km.

basis as a function of the time interval T_c in Fig. 6, which is calculated under the optimal key rate. The distance between Alice and Bob is 300 km and the system repetition rate is $F = 4 \text{ GHz}$. The experimental parameters were set to the typical values given in Table. II. With a fixed frequency difference, the error rate in the X basis increases as the time bin interval increases. When the frequency difference $\delta\nu = 10 \text{ kHz}$, the error rate increases slowly, indicating that a relatively low system repetition rate is sufficient for the experiment.

IV. PERFORMANCE AND DISCUSSION

We numerically simulate the key rate $R = \ell/N$ of our asynchronous-MDIQKD protocol in finite-size cases. We set the threshold $\Lambda = 10$. The genetic algorithm is exploited to globally search for the optimal value of light intensities and their corresponding probabilities. When optimizing the key rate, we set an additional condition in which the mean number of *case 2* events $\bar{N}^{c_2} \leq 1$. Assuming that the distribution of the number of events in

TABLE II. Simulation parameters. η_d and p_d are the detector efficiency and dark count rate, respectively. α is the attenuation coefficient of the fiber and f denotes the error correction efficiency. ϵ is the failure probability considered in the error verification and finite data analysis.

η_d	p_d	α	f	ϵ
70%	10^{-8}	0.165 dB/km	1.1	$36/23 \times 10^{-10}$

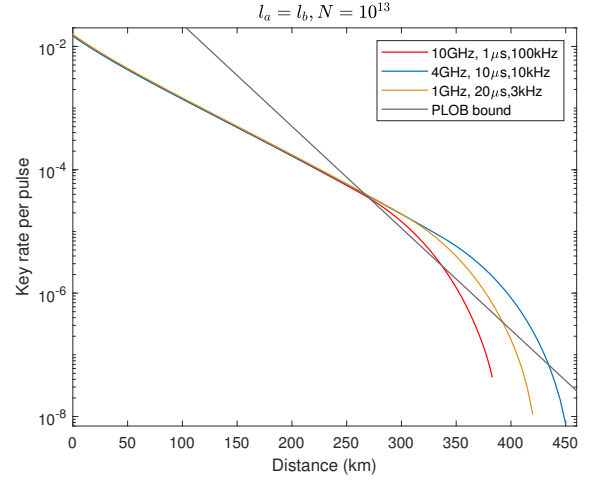


FIG. 8. Secret key rates of our protocol with short-term matching as a function of the distance where both phase tracking and phase locking are not adopted. Different system repetition rates F , matching time intervals T_c and frequency differences $\delta\nu$ are taken into consideration. Red line: $F = 10 \text{ GHz}$, $T_c = 1 \mu\text{s}$, $\delta\nu = 100 \text{ kHz}$; blue line: $F = 4 \text{ GHz}$, $T_c = 10 \mu\text{s}$, $\delta\nu = 10 \text{ kHz}$; yellow line: $F = 1 \text{ GHz}$, $T_c = 20 \mu\text{s}$, $\delta\nu = 3 \text{ kHz}$. Our protocol can overcome the PLOB bound at 270 km with a key rate of 2×10^{-5} .

case 2 follows a Poisson distribution, the probability that the observed number of *case 2* events in the experiment exceeds Λ is $1 - \sum_{k=0}^{\Lambda} \frac{\bar{N}^{c_2 k}}{k!} e^{-\bar{N}^{c_2}} \approx 1 \times 10^{-8}$, where $\varsigma = \bar{N}^{c_2}$. This reveals the robustness of our protocol, which will only fail once in 100 million rounds of experiments.

The experimental parameters were set to the typical values given in Table. II. We set the failure parameters ϵ' , $\hat{\epsilon}$, ϵ_e , ϵ_β , and ϵ_{PA} to be the same ϵ . We denote the distance between Alice (Bob) and Charlie as l_a (l_b). In the symmetric case, that is, $l_a = l_b = l/2$, we have $\epsilon_0 + \epsilon_1 = 14\epsilon$ because the Chernoff bound [89, 90] is used 14 times to estimate $s_{0\mu_b}^z$, s_{11}^z , and e_{11}^x . The corresponding security bound is $\epsilon_{\text{asyn}} = 2.4 \times 10^{-9}$. Similarly, in the asymmetric case, we have $\epsilon_0 + \epsilon_1 = 13\epsilon$ and $\epsilon_{\text{asyn}} = 2.3 \times 10^{-9}$.

First, we calculate the key rates of the asynchronous-MDIQKD protocol with a short time interval T_c . The detailed formulas for simulating our protocol are presented in Appendix B. The statistical fluctuation analysis formulas are presented in Appendix C. Fig. 7 shows a scenario in which phase tracking is removed. The time interval $T_c = 50 \mu\text{s}$, and the system repetition rate is $F = 1 \text{ GHz}$. We assume that the angle of misalignment in the X basis $\sigma = \pi/10$. The key rate beats the PLOB bound at 280 km under the condition where the data size is $N = 10^{12}$ and the transmission distance reaches 450 km. One can also transmit over more than 420 km and overcome the PLOB even with a data size of $N = 10^{11}$.

The key rate in the case where neither phase-tracking nor phase-locking techniques are employed is shown in Fig. 8. Here, we consider the frequency differences of 3,

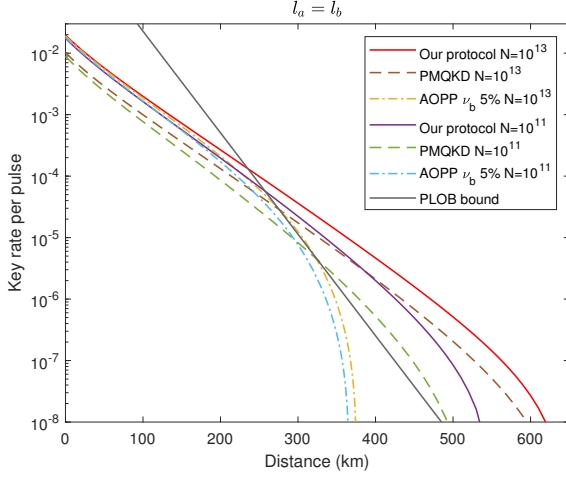


FIG. 9. Comparison of the secret key rates of the asynchronous-MDIQKD with arbitrary-time matching, PMQKD [40] and AOPP [81] in symmetric channels. The numerical results here show that our protocol has a notable advantage and is able to achieve a long transmission distance of 620 km.

10 and 100 kHz. Correspondingly, the system repetition rates are 1 GHz, 4 GHz (which has been employed in the experiments in Ref. [60]) and 10 GHz. Note that when $T_c = 20 \mu\text{s}$, the phase misalignment caused by fiber phase drift is considered. The simulation results show that the proposed protocol can overcome the PLOB bound at 270 km. For the frequency difference $\delta\nu = 100 \text{ kHz}$, by applying a 10 GHz system and setting the matching time interval $T_c = 1 \mu\text{s}$, the secure transmission distance can still exceed 380 km. The corresponding loss is 62 dB. In free space, if the Micius satellite [73] is used as the intermediate station Charlie, the key distribution between two ground nodes with a distance of approximately 1000 km can be realized. At an intercity distance of 300 km, the key rate is 0.15 Mbps, which is sufficient to perform a variety of tasks, including audio and video encryption.

We remark that by circumventing the need for phase tracking, the asynchronous-MDIQKD protocol has a noteworthy advantage over TFQKD at intercity distance. Typically, the maximum counting rate of a commercially available SNSPD is approximately 2 MHz per channel. For TFQKD, using strong reference light to execute phase-tracking usually consumes a count rate of about 4 MHz per channel [50] (sometimes 40 MHz peak count rate [51]), and dedicated high-performance detectors are needed. In Ref. [51], the two-parallel-nanowire serial-connected configuration is developed to address the high count rate issue. In contrast, asynchronous-MDIQKD does not impose a strict count rate requirement on the detector, and all detector count rates are usable for quantum signals. Assuming the maximum counting rate is 5 MHz per channel, at 230 km, with a 4 GHz repetition rate, the count rate of the quantum signal will be approximately 4.4 MHz per channel, which can be used

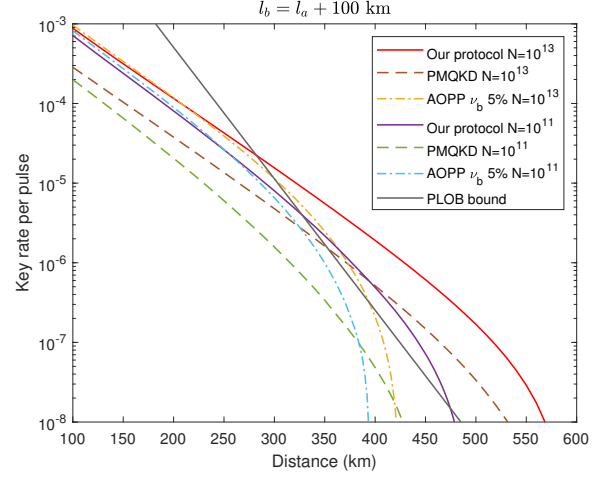


FIG. 10. Comparison of secret key rates of our protocol with arbitrary time matching, PMQKD, and AOPP versus transmission distance in asymmetric channels. Our protocol exhibits a decent performance in asymmetric channels.

for key generation in our protocol. The key rate is 350 kbps when $\delta\nu = 10 \text{ kHz}$ and $T_c = 10 \mu\text{s}$. However, for TFQKD, the available count rate is only 1 MHz per channel, resulting in a key rate of approximately 20 kbps [51]. In this case, the key rate of our protocol is one order of magnitude higher than that of TFQKD.

For a large time interval T_c , say 1 s, the phase correlation between two time bins fades. With the same experimental complexity as TFQKD, that is, using phase locking and phase tracking, one can postmatch time bins with arbitrary time interval and achieve better performance. Here, we simulate the key rates of asynchronous-MDIQKD with arbitrary time matching and compare it with those of PMQKD (PMQKD) [40] and SNSQKD with the help of actively AOPP. We set the total number of pulses as $N = 10^{11}$ and 10^{13} , the misalignment in the X basis as $\sigma = \pi/36$, and the security bounds as $\varepsilon_{\text{AMDI}} = \varepsilon_{\text{AOPP}} = 3.6 \times 10^{-9}$ and $\varepsilon_{\text{PM}} = O(10^{-9})$. The detailed formulas for simulating our protocol are presented in Appendix B.

Because our protocol is an MDI-type protocol, the density matrix of the single-photon pair component is always identical in the X and Z bases for each user, regardless of the asymmetric source parameters chosen. This makes it possible for a dynamic quantum network to add or delete new user nodes without considering the source parameters of existing users. In contrast, to guarantee that the density matrix of the two users' joint single-photon state in the X basis is the same as that in the Z basis for SNSQKD protocols, the transmission probability and intensity of the coherent state must follow strict mathematical constraint [33, 39]. However, this constraint is difficult to realize in practice, especially in networks where users are added and deleted over time, which greatly degrades their performance. By exploiting the quantum coin concept [91, 92], a recent study provided a security

proof for the SNSQKD protocol when the constraint is not satisfied [80]. When comparing the key rates, we considered that the intensity of the coherent state in AOPP does not satisfy the mathematical constraint (which is often the case in practice) with a modulation deviation of decoy state ν_b to 5%, and the other parameters have no deviation. The key rates in symmetric channels are shown in Fig. 9. The simulation results show that the key rate of asynchronous-MDIQKD is always higher than that of PMQKD and AOPP. At 500 km, for $N = 10^{13}$, the secret key rate of our protocol is 150% higher than that of PMQKD, and the transmission distance is 240 km longer than that of AOPP. For $N = 10^{11}$, our protocol transmits over a distance of more than 500 km. Fig. 10 shows the key rate in the asymmetric channels, where $l_b = l_a + 100$ km. Notably, our protocol also performs well in asymmetric channels. At 500 km, for $N = 10^{13}$, the key rate of our protocol is 400% higher than that of PMQKD, and the transmission distance is 150 km longer than that of AOPP. Similarly, when $N = 10^{11}$, the transmission distance of the asynchronous-MDIQKD protocol is 50 km higher.

In summary, the asynchronous-MDIQKD protocol does not require complicated phase-locking and phase-tracking techniques, and it is resistant to imperfect intensity modulation. Therefore, an intercity quantum network is possible, where users can dynamically access and freely choose to perform asynchronous-MDIQKD with short time matching or arbitrary time matching.

V. CONCLUSION

In this work, we presented an asynchronous-MDIQKD protocol through time multiplexing. We realized $O(\sqrt{\eta})$ scaling of the key rate with asynchronous two-photon interference, thus surpassing the PLOB bound. By removing phase locking and phase tracking, our protocol greatly simplifies the hardware requirement with a small sacrifice in performance. When using the same experimental techniques as TFQKD, our protocol is secure against coherent attacks, and shows longer transmission and higher key rate than PMQKD and SNSQKD (AOPP), considering imperfect intensity modulation. Our work also suggests a practical method of overcoming the linear bound of dual-rail protocols [30] without challenging technologies. In addition, our protocol can also exploit the six-state encoding [93] due to random phase modulation. Therefore, if applying single photon sources in the Z basis, our protocol can be made secure up to higher error rate by establishing the non-trivial mutual information between the bit-flip and phase error patterns [93, 94], thereby achieving a higher key rate. This work exhibits remarkable superiority in intercity quantum network deployment for balancing performance and technical complexity. We believe the key contributions of this work will produce exciting opportunities for the widespread deployment of global quantum networks be-

yond quantum key distribution, ranging from quantum repeaters to quantum entanglement distribution.

ACKNOWLEDGMENTS

We gratefully acknowledge the support from the National Natural Science Foundation of China (No. 61801420), the Natural Science Foundation of Jiangsu Province (No. BK20211145), the Fundamental Research Funds for the Central Universities (No. 020414380182), the Key Research and Development Program of Nanjing Jiangbei New Area (No. ZDYD20210101), the Key-Area Research and Development Program of Guangdong Province (No. 2020B0303040001), and the China Postdoctoral Science Foundation (No. 2021M691536).

Note added— During the peer review of our work, we became aware of a similar work by Zeng et al. [95], who consider a mode-pairing MDI-QKD scheme that matches the adjacent detection pulses to extract the key information. By assuming infinite decoy states, they calculated the key rate in the asymptotic regime, which can break the rate-loss bound. In this work, we use the three-intensity decoy-state method to calculate the key rate in the finite-size regime and show its ability to break the rate-loss bound.

Appendix A: Simulation formulas

In this section, we calculate the parameters in Eq. (1) to estimate the secret key rate. In the following description, let x^* be the expected value of x . We denote the number of $\{k_a, k_b\}$ as $x_{k_a k_b}$. We denote the number and error number of events $\{k_a^i k_b^j, k_b^i k_a^j\}$ after postmatching as $n_{k_a^i k_b^j, k_b^i k_a^j}$ and $m_{k_a^i k_b^j, k_b^i k_a^j}$, respectively. For simplicity, we abbreviate $k_a^i k_b^j, k_b^i k_a^j$ as $2k_a, 2k_b$ when $k_a^i = k_b^j$ and $k_b^i = k_a^j$.

1. s_{11}^* . s_{11}^* corresponds to the number of successful detection events where Alice and Bob each emit a single photon in different time bins in the Z basis. We define z_{10} (z_{01}) as the number of events in which Alice (Bob) emits a single photon and Bob (Alice) emits a vacuum state in $\{\mu_a, \mathbf{o}_b\}$ ($\{\mathbf{o}_a, \mu_b\}$) event. The lower bounds of their expected values are $\underline{z}_{10}^* = N p_{\mu_a} p_{\mathbf{o}_b} \mu_a e^{-\mu_a} \underline{y}_{10}^*$ and $\underline{z}_{01}^* = N p_{\mathbf{o}_a} p_{\mu_b} \mu_b e^{-\mu_b} \underline{y}_{01}^*$, where the yields \underline{y}_{10}^* and \underline{y}_{01}^* are the corresponding yields. These can be estimated using the decoy-state method:

$$\underline{y}_{01}^* \geq \frac{\mu_b}{N(\mu_b \nu_b - \nu_b^2)} \left(\frac{e^{\nu_b} \underline{x}_{\mathbf{o}_a \nu_b}^*}{p_{\mathbf{o}_a} p_{\nu_b}} - \frac{\nu_b^2}{\mu_b^2} \frac{e^{\mu_b} \underline{x}_{\mathbf{o}_a \mu_b}^*}{p_{\mathbf{o}_a} p_{\mu_b}} - \frac{\mu_b^2 - \nu_b^2}{\mu_b^2} \frac{\underline{x}_{\mathbf{o}_a \mathbf{o}_b}^{d*}}{p_{\mathbf{o}_a \mathbf{o}_b}^d} \right), \quad (\text{A1})$$

$$\underline{y}_{10}^* \geq \frac{\mu_a}{N(\mu_a \nu_a - \nu_a^2)} \left(\frac{e^{\nu_a} \underline{x}_{\nu_a \mathbf{o}_b}^*}{p_{\nu_a} p_{\mathbf{o}_b}} - \frac{\nu_a^2}{\mu_a^2} \frac{e^{\mu_a} \underline{x}_{\mu_a \mathbf{o}_b}^*}{p_{\mu_a} p_{\mathbf{o}_b}} - \frac{\mu_a^2 - \nu_a^2}{\mu_a^2} \frac{\underline{x}_{\mathbf{o}_a \mathbf{o}_b}^{d*}}{p_{\mathbf{o}_a \mathbf{o}_b}^d} \right), \quad (\text{A2})$$

where $x_{oo}^d = x_{\hat{o}_a \hat{o}_b} + x_{\hat{o}_a o_b} + x_{o_a \hat{o}_b}$ represents the number of events where at least one user chooses the declare-vacuum state and $p_{oo}^d = p_{\hat{o}_a \hat{o}_b} + p_{\hat{o}_a o_b} + p_{o_a \hat{o}_b}$ refers to the corresponding probability. Thus, the lower bound of s_{11}^{z*} can be given by

$$\underline{s}_{11}^{z*} = n_C^z \frac{\underline{z}_{10}^*}{x_{\mu_a o_b}} \frac{\underline{z}_{01}^*}{x_{o_a \mu_b}} = \frac{\underline{z}_{10}^* \underline{z}_{01}^*}{x_{\max}}. \quad (\text{A3})$$

where $x_0 = x_{o_a \mu_b} + x_{o_a o_b}$, $x_1 = x_{\mu_a o_b} + x_{\mu_a \mu_b}$ and $x_{\max} = \max\{x_0, x_1\}$.

2. $\underline{s}_{0\mu_b}^{z*}$. $\underline{s}_{0\mu_b}^{z*}$ represents the number of events in the Z basis, Alice emits a zero-photon state in the two matched time bins, and the total intensity of Bob's pulses is μ_b . We define z_{00} ($z_{0\mu_b}$) as the number of detection events where the state sent by Alice collapses to the vacuum state in the $\{\mu_a, o_b\}$ ($\{\mu_a, \mu_b\}$) event. The lower bounds of the expected values are $\underline{z}_{00}^* = p_{\mu_a} p_{o_b} e^{-\mu_a} \underline{x}_{oo}^{d*} / p_{oo}^d$ and $\underline{z}_{0\mu_b}^* = p_{\mu_a} p_{\mu_b} e^{-\mu_a} \underline{x}_{o_a \mu_b}^* / p_{o_a} p_{\mu_b}$, respectively. In this study, we employed the relation between the expected value $\underline{x}_{o_a \mu_b}^* = p_{o_a} \underline{x}_{\hat{o}_a \mu_b}^* / p_{\hat{o}_a}$, and $\underline{x}_{o_a o_b}^* = p_{o_a} p_{o_b} \underline{x}_{oo}^{d*} / p_{oo}^d$. The lower bound of $\underline{s}_{0\mu_b}^{z*}$ can be written as

$$\underline{s}_{0\mu_b}^{z*} = n_C^z \frac{\underline{z}_{00}^*}{x_{\mu_a o_b}^*} + n_E^z \frac{\underline{z}_{0\mu_b}^*}{x_{\mu_a \mu_b}^*}, \quad (\text{A4})$$

3. \underline{s}_{11}^{x*} . The phase difference between Alice and Bob is defined as $\varphi = \theta_a - \theta_b + \phi$ and the corresponding number in the $\{k_a, k_b\}$ event as $x_{k_a k_b}^\varphi$. In the post-matching step, two time bins are matched if they have the same phase difference φ , and all $\{2\nu_a, 2\nu_b\}$ events can be grouped according to the phase difference φ . We denote the number of $\{2\nu_a, 2\nu_b\}$ events with phase difference φ as $n_{2\nu_a, 2\nu_b}^\varphi = x_{2\nu_a, 2\nu_b}^\varphi / 2$. Similar to the time-bin MDIQKD, the expected yields of single-photon pairs in the X and Z bases satisfy the following relation:

$$\begin{aligned} Y_{11}^{x*} &= Y_{11}^{z*} = \frac{1}{4} (y_{01}^* y_{10}^* + y_{10}^* y_{01}^* + y_{00}^* y_{11}^* + y_{11}^* y_{00}^*) \\ &\geq \frac{1}{2} y_{10}^* y_{01}^*. \end{aligned} \quad (\text{A5})$$

Suppose the global phase difference φ is a randomly and uniformly distributed value. The expected number of single-photon pairs can be given by

$$\begin{aligned} s_{11}^{x*} &= \frac{1}{2\pi} \int_0^{2\pi} n_{2\nu_a, 2\nu_b}^\varphi \times \frac{4\nu_a \nu_b e^{-2\nu_a - 2\nu_b}}{q_{\nu_a \nu_b}^\varphi q_{\nu_a \nu_b}^\varphi} y_{11}^{x*} d\varphi \\ &\geq \frac{1}{2\pi} \int_0^{2\pi} n_{2\nu_a, 2\nu_b}^\varphi \times \frac{\nu_a \nu_b e^{-2\nu_a - 2\nu_b}}{q_{\nu_a \nu_b}^\varphi q_{\nu_a \nu_b}^\varphi} 2y_{10}^* y_{01}^* d\varphi \\ &= N p_{\nu_a} p_{\nu_b} \nu_a \nu_b e^{-2(\nu_a + \nu_b)} \frac{y_{10}^* y_{01}^*}{2\pi q_{\nu_a \nu_b}^\varphi} \int_0^{2\pi} \frac{1}{2\pi q_{\nu_a \nu_b}^\varphi} d\varphi, \end{aligned} \quad (\text{A6})$$

where the coefficient 4 on the first line of the formula corresponds to the four modes of single-photon pairs in the X basis, $q_{\nu_a \nu_b}^\varphi$ is the gain when Alice chooses intensity ν_a , and Bob chooses intensity ν_b with phase difference φ and $n_{2\nu_a, 2\nu_b}^\varphi = N p_{\nu_a} p_{\nu_b} q_{\nu_a \nu_b}^\varphi / 2$. We define

$q_{k_a k_b} = 1/(2\pi) \int_0^{2\pi} q_{k_a k_b}^\varphi d\varphi$ as the average gain, given that Alice chooses intensity k_a , and Bob chooses intensity k_b . When ν_a and $\nu_b \approx 0$, there is an approximation relation $\int_0^{2\pi} 1/(2\pi q_{\nu_a \nu_b}^\varphi) d\varphi \approx 1/q_{\nu_a \nu_b}$.

In the discrete case, the phase difference φ is divided into M slices $\{\delta_m\}$ for $1 \leq m \leq M$, where m is an integer, where $\delta_m = [2\pi(m-1)/M, 2\pi m/M)$. The expected number of single-photon pairs is given by

$$\underline{s}_{11}^{x*} \geq \sum_{m=1}^M n_{2\nu_a, 2\nu_b}^m \times 2 \frac{\nu_a e^{-\nu_a - \nu_b} \underline{y}_{10}^*}{q_{\nu_a \nu_b}^m} \frac{\nu_b e^{-\nu_a - \nu_b} \underline{y}_{01}^*}{q_{\nu_a \nu_b}^m}, \quad (\text{A7})$$

where $n_{2\nu_a, 2\nu_b}^m$ is the number of $\{2\nu_a, 2\nu_b\}$ events with phase difference φ falling into slice δ_m . $q_{\nu_a \nu_b}^m$ is the corresponding gain.

4. \bar{e}_{11}^{x*} . For single-photon pairs, the expected value of the phase error rate in the Z basis equals the expected value of the bit error rate in the X basis, and the error rate $\bar{e}_{11}^{x*} = \bar{t}_{11}^x / \underline{s}_{11}^{x*}$. Therefore, we first calculate the number of errors of the single-photon pairs in the X basis t_{11}^x . The upper bound of t_{11}^x can be expressed as

$$\bar{t}_{11}^x \leq m_{2\nu_a, 2\nu_b} - (\underline{m}_{0, 2\nu_b} + \underline{m}_{2\nu_a, 0}) + \bar{m}_{0,0}, \quad (\text{A8})$$

where $m_{0, 2\nu_b}$ ($m_{2\nu_a, 0}$) is the error count when the state sent by Alice (Bob) collapses to the vacuum state in events $\{2\nu_a, 2\nu_b\}$, and $\bar{m}_{0,0}$ corresponds to the event where the states sent by Alice and Bob both collapse to vacuum states in events $\{2\nu_a, 2\nu_b\}$. The expected error counts $m_{0, 2\nu_b}^*$ and $m_{2\nu_a, 0}^*$ can be expressed as follows:

$$\begin{aligned} m_{0, 2\nu_b}^* &= e_o \frac{1}{2\pi} \int_0^{2\pi} n_{2\nu_a, 2\nu_b}^\varphi \frac{e^{-\nu_a} q_{0\nu_b}^*}{q_{\nu_a \nu_b}^\varphi} \frac{e^{-\nu_a} q_{0\nu_b}^*}{q_{\nu_a \nu_b}^\varphi} d\varphi \\ &= e_o N p_{\nu_a} p_{\nu_b} e^{-2\nu_a} q_{0\nu_b}^{*2} \frac{1}{4\pi} \int_0^{2\pi} \frac{1}{q_{\nu_a \nu_b}^\varphi} d\varphi, \\ m_{2\nu_a, 0}^* &= e_o \frac{1}{2\pi} \int_0^{2\pi} n_{2\nu_a, 2\nu_b}^\varphi \frac{e^{-\nu_b} q_{\nu_a 0}^*}{q_{\nu_a \nu_b}^\varphi} \frac{e^{-\nu_b} q_{\nu_a 0}^*}{q_{\nu_a \nu_b}^\varphi} d\varphi \\ &= e_o N p_{\nu_a} p_{\nu_b} e^{-2\nu_b} q_{\nu_a 0}^{*2} \frac{1}{4\pi} \int_0^{2\pi} \frac{1}{q_{\nu_a \nu_b}^\varphi} d\varphi, \end{aligned} \quad (\text{A9})$$

respectively, where $e_o = 1/2$ is the error rate of the background noise.

In the symmetric case, $\nu_a = \nu_b$, $p_{o_a} = p_{o_b}$, and $p_{\nu_a} = p_{\nu_b}$. In this case, we have $q_{\nu_a o}^* = q_{o \nu_b}^* = (x_{o_a \nu_b} + x_{\nu_a o_b})^* / (2N p_{o_a} p_{\nu_b})$. In the asymmetric case, $q_{\nu_a o}^* = x_{\nu_a o_b}^* / (N p_{\nu_a} p_{o_b})$ and $q_{o \nu_b}^* = x_{o_a \nu_b}^* / (N p_{o_a} p_{\nu_b})$. Then, the lower bound of the observed value of $m_{0, 2\nu_b} + m_{2\nu_a, 0}$ can be written as

$$\underline{m}_{0, 2\nu_b} + \underline{m}_{2\nu_a, 0} = \varphi^L(\underline{m}_{0, 2\nu_b}^* + \underline{m}_{2\nu_a, 0}^*, \epsilon). \quad (\text{A10})$$

where $\varphi^L(x)$ is the lower bounds when using Chernoff bound to estimate the real values according to the expected values and is defined in Eq. C1. The expected

value of $m_{0,0}$ can be given by

$$\begin{aligned} m_{0,0}^* &= e_o \frac{1}{2\pi} \int_0^{2\pi} n_{2\nu_a, 2\nu_b}^\varphi \frac{e^{-\nu_a - \nu_b} q_{00}^*}{q_{\nu_a \nu_b}^\varphi} \frac{e^{-\nu_a - \nu_b} q_{00}^*}{q_{\nu_a \nu_b}^\varphi} d\varphi \\ &= e_o N p_{\nu_a} p_{\nu_b} e^{-2(\nu_a + \nu_b)} q_{00}^{*2} \frac{1}{4\pi} \int_0^{2\pi} \frac{1}{q_{\nu_a \nu_b}^\varphi} d\varphi. \end{aligned} \quad (\text{A11})$$

The upper bound of q_{00}^* can be obtained from $\bar{q}_{00}^* = \bar{m}_{oo}^{d*}/(Np_{oo}^d)$. The upper bound of $m_{0,0}$ can be obtained by $\bar{m}_{0,0} = \varphi^U(\bar{m}_{0,0}^*, \epsilon)$, where $\varphi^U(x)$ is the upper bound while using the Chernoff bound to estimate the observed values according to the expected values and is defined in Eq. C2.

5. $\bar{\phi}_{11}^z$. Finally, for a failure probability ϵ , the upper bound of the phase error rate $\bar{\phi}_{11}^z$ can be obtained by using random sampling without replacement in Eq. (C5)

$$\bar{\phi}_{11}^z \leq \bar{e}_{11}^x + \gamma(\underline{s}_{11}^z, \underline{s}_{11}^x, \bar{e}_{11}^x, \epsilon). \quad (\text{A12})$$

Appendix B: Simulation details

1. Asynchronous-MDIQKD protocol for arbitrary-time matching

Similar to the time-bin encoding MDIQKD, the valid events after postmatching in the Z basis can be divided into correct events $\{\mu_a \mathbf{o}_a, \mathbf{o}_b \mu_b\}$, $\{\mathbf{o}_a \mu_a, \mu_b \mathbf{o}_b\}$, and incorrect events $\{\mu_a \mathbf{o}_a, \mu_b \mathbf{o}_b\}$, $\{\mathbf{o}_a \mu_a, \mathbf{o}_b \mu_b\}$. The corresponding numbers are denoted as n_C^z and n_E^z , respectively, which can be written as

$$n_C^z = x_{\min} \frac{x_{\mathbf{o}_a \mu_b} x_{\mu_a \mathbf{o}_b}}{x_0 x_1} = \frac{x_{\mathbf{o}_a \mu_b} x_{\mu_a \mathbf{o}_b}}{x_{\max}},$$

and

$$n_E^z = x_{\min} \frac{x_{\mathbf{o}_a \mathbf{o}_b} x_{\mu_a \mu_b}}{x_0 x_1} = \frac{x_{\mathbf{o}_a \mathbf{o}_b} x_{\mu_a \mu_b}}{x_{\max}},$$

where $x_{\min} = \min\{x_0, x_1\}$. The overall number of events in the Z basis is $n^z = n_C^z + n_E^z$ and the bit error rate in the Z basis is $E^z = n_E^z/n^z$.

In the X basis, the data are composed of events $\{2\nu_a, 2\nu_b\}$, $\{2\mathbf{o}_a, 2\nu_b\}$, $\{2\nu_a, 2\mathbf{o}_b\}$, $\{2\hat{\mathbf{o}}_a, 2\mathbf{o}_b\}$, and $\{2\mathbf{o}_a, 2\hat{\mathbf{o}}_b\}$. Without loss of generality, we consider the case in which all matched events satisfy $\theta_a^i - \theta_a^j - (\theta_b^i - \theta_b^j) + (\phi^i - \phi^j) = 0$. In this case, when $r_a^i \oplus r_a^j \oplus r_b^i \oplus r_b^j = 0$ (1), the $\{\nu_a^i \nu_b^j, \nu_b^i \nu_a^j\}$ event is considered to be an error event when different detectors (the same detector) click at time bins i and j .

When Alice and Bob send intensities k_a and k_b with phase difference φ , the gain corresponding to only one detector click is

$$\begin{aligned} q_{k_a k_b}^{L\varphi} &= y_{k_a k_b} [e^{\omega_{k_a k_b} \cos \varphi} - y_{k_a k_b}], \\ q_{k_a k_b}^{R\varphi} &= y_{k_a k_b} [e^{-\omega_{k_a k_b} \cos \varphi} - y_{k_a k_b}]. \end{aligned} \quad (\text{B1})$$

where $y_{k_a k_b} := e^{\frac{-(\eta_a k_a + \eta_b k_b)}{2}} (1 - p_d)$, $\omega_{k_a k_b} := \sqrt{\eta_a k_a \eta_b k_b}$, $\eta_a = \eta_d 10^{-\alpha_{la}/10}$ and $\eta_b = \eta_d 10^{-\alpha_{lb}/10}$. The overall gain can be given by $q_{k_a k_b} = 1/2\pi \int_0^{2\pi} q_{k_a k_b}^\varphi d\varphi = 1/2\pi \int_0^{2\pi} (q_{k_a k_b}^{L\varphi} + q_{k_a k_b}^{R\varphi}) d\varphi = 2y_{k_a k_b} [I_0(\omega_{k_a k_b}) - y_{k_a k_b}]$, where $I_0(x)$ represents the zero-order modified Bessel function of the first kind. The total number of $\{k_a, k_b\}$ is $x_{k_a k_b} = N p_{k_a} p_{k_b} q_{k_a k_b}$.

The overall error count in the X basis can be given as

$$\begin{aligned} m_{2\nu_a, 2\nu_b} &= \frac{1}{2\pi} \int_0^{2\pi} n_{2\nu_a, 2\nu_b}^\varphi \left[\frac{q_{\nu_a \nu_b}^{L\varphi} q_{\nu_a \nu_b}^{R(\varphi+\sigma)} + q_{\nu_a \nu_b}^{R\varphi} q_{\nu_a \nu_b}^{L(\varphi+\sigma)}}{q_{\nu_a \nu_b}^{\varphi+\sigma}} \right] d\varphi \\ &= N p_{\nu_a} p_{\nu_b} \frac{1}{4\pi} \int_0^{2\pi} \frac{q_{\nu_a \nu_b}^{L\varphi} q_{\nu_a \nu_b}^{R(\varphi+\sigma)} + q_{\nu_a \nu_b}^{R\varphi} q_{\nu_a \nu_b}^{L(\varphi+\sigma)}}{q_{\nu_a \nu_b}^{\varphi+\sigma}} d\varphi. \end{aligned} \quad (\text{B2})$$

where σ refers to the angle of misalignment in the X basis.

2. Asynchronous-MDIQKD protocol for short-term matching

The total number of time bins per T_c is $N_{T_c} = T_c F$. For each detection event, the probability that it belongs to *case 1* is $p_{c1} = 1 - (1 - \bar{p})^{2N_{T_c}-2}$ and the probability of belonging to *case 2* is $p_{c2} = (1 - \bar{p})^{2N_{T_c}-2}$, where $\bar{p} = \sum_{k_a, k_b} p_{k_a} p_{k_b} q_{k_a k_b}$ is the average detection probability, and $2N_{T_c} - 2$ is the total number of time bins neighboring the given detection event. The mean number of *case 2* events is $\bar{N}^{c2} = N p_{c2} \bar{p}$.

For simplicity, we divide the post-matching window into d windows with a time length of T_c , where $d = N/N_{T_c}$. In the Z basis, given that Alice sends k_a and Bob sends k_b , the detection count in the i -th window and the total detection count are $x_{k_a k_b}^i = N_{T_c} p_{c1} p_{k_a} p_{k_b} q_{k_a k_b}$ and $x_{k_a k_b} = N p_{c1} p_{k_a} p_{k_b} q_{k_a k_b}$, respectively. After post-matching, the number of correct and incorrect events in the Z basis is

$$\begin{aligned} n_C^z &= \sum_{i=1}^d x_{\min}^i \frac{x_{\mathbf{o}_a \mu_b}^i x_{\mu_a \mathbf{o}_b}^i}{x_0^i x_1^i} = \sum_{i=1}^d \frac{x_{\mu_a \mathbf{o}_b}^i x_{\mathbf{o}_a \mu_b}^i}{x_{\max}^i}, \\ n_E^z &= \sum_{i=1}^d x_{\min}^i \frac{x_{\mathbf{o}_a \mathbf{o}_b}^i x_{\mu_a \mu_b}^i}{x_0^i x_1^i} = \sum_{i=1}^d \frac{x_{\mathbf{o}_a \mathbf{o}_b}^i x_{\mu_a \mu_b}^i}{x_{\max}^i}, \end{aligned}$$

respectively, where $x_0^i = x_{\mathbf{o}_a \mu_b}^i + x_{\mathbf{o}_a \mathbf{o}_b}^i$, $x_1^i = x_{\mu_a \mathbf{o}_b}^i + x_{\mu_a \mu_b}^i$, $x_{\min}^i = \min\{x_0^i, x_1^i\}$, $x_{\max}^i = \max\{x_0^i, x_1^i\}$. The overall number of events in the Z basis is $n^z = n_C^z + n_E^z$, and the bit error rate in the Z basis is $E^z = n_E^z/n^z$.

In our simulation, we set $M = 16$. Assuming that $x_{\nu_a \nu_b}^m$, the detection count of $\{\nu_a, \nu_b\}$ events in slice δ_m follows the Poisson distribution $P_r(x_{\nu_a \nu_b}^m = j) = \frac{\lambda^j}{j!} e^{-\lambda}$, where $\lambda = \bar{x}_{\nu_a \nu_b}^i$ is the mean value of $x_{\nu_a \nu_b}^m$. In the post-matching step, if $x_{\nu_a \nu_b}^m$ is even, all $\{\nu_a, \nu_b\}$ events within the m -th T_c will be utilized. If $x_{\nu_a \nu_b}^m$ is odd, there will be a redundant $\{\nu_a, \nu_b\}$ event to be aborted. Therefore,

the mean number of $\{2\nu_a, 2\nu_b\}$ events per T_c is

$$n_{2\nu_a, 2\nu_b}^i = \frac{2}{M} \left[\sum_k^{\left\lfloor \frac{N_{T_c}-1}{2} \right\rfloor} k P_r(2k) + k P_r(2k+1) \right] \quad (\text{B3})$$

$$= \frac{1}{M} \left[\lambda - \frac{1 - e^{-2\lambda}}{2} \right].$$

The overall error count in the X basis can be given as

$$m_{2\nu_a, 2\nu_b}^i = n_{2\nu_a, 2\nu_b}^i \sum_{m=0}^{\frac{M}{2}-1} \left[\frac{2}{M} \frac{q_{\nu_a \nu_b}^{L\varphi_m} q_{\nu_a \nu_b}^{R(\varphi_m+\sigma)} + q_{\nu_a \nu_b}^{R\varphi_m} q_{\nu_a \nu_b}^{L(\varphi_m+\sigma)}}{q_{\nu_a \nu_b}^{\varphi_m} q_{\nu_a \nu_b}^{\varphi_m+\sigma}} \right], \quad (\text{B4})$$

where $\varphi_m = 2\pi m/M$.

Appendix C: Statistical fluctuation analysis

In this Appendix, we introduce the statistical fluctuation analysis method [90] used in the simulation.

Chernoff bound. Let x^* be the expected value of x . For a given expected value x^* , the Chernoff bound can be used to obtain the upper and lower bounds of the observed value.

$$\bar{x} = \varphi^U(x^*) = x^* + \frac{\beta}{2} + \sqrt{2\beta x^* + \frac{\beta^2}{4}}, \quad (\text{C1})$$

and

$$\underline{x} = \varphi^L(x^*) = x^* - \sqrt{2\beta x^*}, \quad (\text{C2})$$

where $\beta = \ln \epsilon^{-1}$.

Variant of Chernoff bound. For a given observed value x and failure probability ϵ , the upper and lower bounds of x^* can be acquired by the variant of the Chernoff bound

$$\bar{x}^* = x + \beta + \sqrt{2\beta x + \beta^2}, \quad (\text{C3})$$

and

$$\underline{x}^* = \max \left\{ x - \frac{\beta}{2} - \sqrt{2\beta x + \frac{\beta^2}{4}}, 0 \right\}. \quad (\text{C4})$$

Random sampling without replacement. Let $X_{n+k} := \{x_1, x_2, \dots, x_{n+k}\}$ be a string of binary bits of size $n+k$, where the number of bits is unknown. Let X_k be a random sample (without replacement) bit string with k is picked from X_{n+k} . Let λ be the probability of a bit value 1 observed in X_k . Let X_n be the remaining bit string, where the probability of bit value 1 observed in X_n is χ . The upper bound of χ can be expressed as

$$\bar{\chi} \leq \lambda + \gamma^U(n, k, \lambda, \epsilon), \quad (\text{C5})$$

where

$$\gamma^U(n, k, \lambda, \epsilon) = \frac{\frac{(1-2\lambda)AG}{n+k} + \sqrt{\frac{A^2 G^2}{(n+k)^2} + 4\lambda(1-\lambda)G}}{2 + 2\frac{A^2 G}{(n+k)^2}}, \quad (\text{C6})$$

with $A = \max\{n, k\}$ and $G = \frac{n+k}{nk} \ln \frac{n+k}{2\pi nk\lambda(1-\lambda)\epsilon^2}$.

-
- [1] C. H. Bennett and G. Brassard, Quantum cryptography: Public key distribution and coin tossing, *Theor. Comput. Sci.* **560**, 7 (2014).
 - [2] A. K. Ekert, Quantum cryptography based on bell's theorem, *Phys. Rev. Lett.* **67**, 661 (1991).
 - [3] Y. Zhao, C.-H. F. Fung, B. Qi, C. Chen, and H.-K. Lo, Quantum hacking: Experimental demonstration of time-shift attack against practical quantum-key-distribution systems, *Phys. Rev. A* **78**, 042333 (2008).
 - [4] L. Lydersen, C. Wiechers, C. Wittmann, D. Elser, J. Skaar, and V. Makarov, Hacking commercial quantum cryptography systems by tailored bright illumination, *Nat. Photonics* **4**, 686 (2010).
 - [5] Y.-L. Tang, H.-L. Yin, X. Ma, C.-H. F. Fung, Y. Liu, H.-L. Yong, T.-Y. Chen, C.-Z. Peng, Z.-B. Chen, and J.-W. Pan, Source attack of decoy-state quantum key distribution using phase information, *Phys. Rev. A* **88**, 022308 (2013).
 - [6] F. Xu, X. Ma, Q. Zhang, H.-K. Lo, and J.-W. Pan, Secure quantum key distribution with realistic devices, *Rev. Mod. Phys.* **92**, 025002 (2020).
 - [7] S. Pirandola, U. L. Andersen, L. Banchi, M. Berta, D. Bunandar, R. Colbeck, D. Englund, T. Gehring, C. Lupo, C. Ottaviani, *et al.*, *Advances in quantum cryptography*, *Adv. Opt. Photon.* **12**, 1012 (2020).
 - [8] H.-K. Lo, M. Curty, and B. Qi, Measurement-device-independent quantum key distribution, *Phys. Rev. Lett.* **108**, 130503 (2012).
 - [9] S. L. Braunstein and S. Pirandola, Side-channel-free quantum key distribution, *Phys. Rev. Lett.* **108**, 130502 (2012).
 - [10] Y. Liu, T.-Y. Chen, L.-J. Wang, H. Liang, G.-L. Shentu, J. Wang, K. Cui, H.-L. Yin, N.-L. Liu, L. Li, X. Ma, J. S. Pelc, M. M. Fejer, C.-Z. Peng, Q. Zhang, and J.-W. Pan, Experimental measurement-device-independent quantum key distribution, *Phys. Rev. Lett.* **111**, 130502 (2013).
 - [11] A. Rubenok, J. A. Slater, P. Chan, I. Lucio-Martinez, and W. Tittel, Real-world two-photon interference and proof-of-principle quantum key distribution immune to detector attacks, *Phys. Rev. Lett.* **111**, 130501 (2013).
 - [12] Y.-H. Zhou, Z.-W. Yu, and X.-B. Wang, Making the decoy-state measurement-device-independent quantum key distribution practically useful, *Phys. Rev. A* **93**, 042324 (2016).
 - [13] Z. Tang, Z. Liao, F. Xu, B. Qi, L. Qian, and H.-K. Lo, Experimental demonstration of polarization encoding measurement-device-independent quantum key distribu-

- tion, Phys. Rev. Lett. **112**, 190503 (2014).
- [14] Y. Fu, H.-L. Yin, T.-Y. Chen, and Z.-B. Chen, Long-distance measurement-device-independent multi-party quantum communication, Phys. Rev. Lett. **114**, 090501 (2015).
 - [15] M. Curty, F. Xu, W. Cui, C. C. W. Lim, K. Tamaki, and H.-K. Lo, Finite-key analysis for measurement-device-independent quantum key distribution, Nat. Commun. **5**, 3732 (2014).
 - [16] H.-L. Yin, W.-F. Cao, Y. Fu, Y.-L. Tang, Y. Liu, T.-Y. Chen, and Z.-B. Chen, Long-distance measurement-device-independent quantum key distribution with coherent-state superpositions, Opt. Lett. **39**, 5451 (2014).
 - [17] L. Comandar, M. Lucamarini, B. Fröhlich, J. Dynes, A. Sharpe, S.-B. Tam, Z. Yuan, R. Penty, and A. Shields, Quantum key distribution without detector vulnerabilities using optically seeded lasers, Nat. Photonics **10**, 312 (2016).
 - [18] H.-L. Yin, T.-Y. Chen, Z.-W. Yu, H. Liu, L.-X. You, Y.-H. Zhou, S.-J. Chen, Y. Mao, M.-Q. Huang, W.-J. Zhang, H. Chen, M. J. Li, D. Nolan, F. Zhou, X. Jiang, Z. Wang, Q. Zhang, X.-B. Wang, and J.-W. Pan, Measurement-device-independent quantum key distribution over a 404 km optical fiber, Phys. Rev. Lett. **117**, 190501 (2016).
 - [19] H. Semenenko, P. Sibson, A. Hart, M. G. Thompson, J. G. Rarity, and C. Erven, Chip-based measurement-device-independent quantum key distribution, Optica **7**, 238 (2020).
 - [20] H.-L. Yin, W.-L. Wang, Y.-L. Tang, Q. Zhao, H. Liu, X.-X. Sun, W.-J. Zhang, H. Li, I. V. Puthoor, L.-X. You, *et al.*, Experimental measurement-device-independent quantum digital signatures over a metropolitan network, Phys. Rev. A **95**, 042338 (2017).
 - [21] K. Wei, W. Li, H. Tan, Y. Li, H. Min, W.-J. Zhang, H. Li, L. You, Z. Wang, X. Jiang, T.-Y. Chen, S.-K. Liao, C.-Z. Peng, F. Xu, and J.-W. Pan, High-speed measurement-device-independent quantum key distribution with integrated silicon photonics, Phys. Rev. X **10**, 031030 (2020).
 - [22] R. I. Woodward, Y. Lo, M. Pittaluga, M. Minder, T. Páriso, M. Lucamarini, Z. Yuan, and A. Shields, Gigahertz measurement-device-independent quantum key distribution using directly modulated lasers, npj Quantum Inf. **7**, 58 (2021).
 - [23] C. Wang, Z.-Q. Yin, S. Wang, W. Chen, G.-C. Guo, and Z.-F. Han, Measurement-device-independent quantum key distribution robust against environmental disturbances, Optica **4**, 1016 (2017).
 - [24] X. Zheng, P. Zhang, R. Ge, L. Lu, G. He, Q. Chen, F. Qu, L. Zhang, X. Cai, Y. Lu, S. Zhu, P. Wu, and X.-S. Ma, Heterogeneously integrated, superconducting silicon-photonics platform for measurement-device-independent quantum key distribution, Adv. Photonics **3**, 055002 (2021).
 - [25] Y.-L. Tang, H.-L. Yin, Q. Zhao, H. Liu, X.-X. Sun, M.-Q. Huang, W.-J. Zhang, S.-J. Chen, L. Zhang, L.-X. You, Z. Wang, Y. Liu, C.-Y. Lu, X. Jiang, X. Ma, Q. Zhang, T.-Y. Chen, and J.-W. Pan, Measurement-device-independent quantum key distribution over untrusted metropolitan network, Phys. Rev. X **6**, 011024 (2016).
 - [26] S. Pirandola, R. García-Patrón, S. L. Braunstein, and S. Lloyd, Direct and reverse secret-key capacities of a quantum channel, Phys. Rev. Lett. **102**, 050503 (2009).
 - [27] M. Takeoka, S. Guha, and M. M. Wilde, Fundamental rate-loss tradeoff for optical quantum key distribution, Nat. Commun. **5**, 5235 (2014).
 - [28] S. Pirandola, R. Laurenza, C. Ottaviani, and L. Banchi, Fundamental limits of repeaterless quantum communications, Nat. Commun. **8**, 15043 (2017).
 - [29] S. Pirandola, End-to-end capacities of a quantum communication network, Commun. Phys. **2**, 51 (2019).
 - [30] S. Das, S. Bäuml, M. Winczewski, and K. Horodecki, Universal limitations on quantum key distribution over a network, Phys. Rev. X **11**, 041016 (2021).
 - [31] M. Lucamarini, Z. L. Yuan, J. F. Dynes, and A. J. Shields, Overcoming the rate-distance limit of quantum key distribution without quantum repeaters, Nature **557**, 400 (2018).
 - [32] X. Ma, P. Zeng, and H. Zhou, Phase-matching quantum key distribution, Phys. Rev. X **8**, 031043 (2018).
 - [33] X.-B. Wang, Z.-W. Yu, and X.-L. Hu, Twin-field quantum key distribution with large misalignment error, Phys. Rev. A **98**, 062323 (2018).
 - [34] H.-L. Yin and Y. Fu, Measurement-device-independent twin-field quantum key distribution, Sci. Rep. **9**, 3045 (2019).
 - [35] J. Lin and N. Lütkenhaus, Simple security analysis of phase-matching measurement-device-independent quantum key distribution, Phys. Rev. A **98**, 042332 (2018).
 - [36] M. Curty, K. Azuma, and H.-K. Lo, Simple security proof of twin-field type quantum key distribution protocol, npj Quantum Inf. **5**, 64 (2019).
 - [37] C. Cui, Z.-Q. Yin, R. Wang, W. Chen, S. Wang, G.-C. Guo, and Z.-F. Han, Twin-field quantum key distribution without phase postselection, Phys. Rev. Applied **11**, 034053 (2019).
 - [38] H.-L. Yin and Z.-B. Chen, Coherent-state-based twin-field quantum key distribution, Sci. Rep. **9**, 14918 (2019).
 - [39] X.-L. Hu, C. Jiang, Z.-W. Yu, and X.-B. Wang, Sending-or-not-sending twin-field protocol for quantum key distribution with asymmetric source parameters, Phys. Rev. A **100**, 062337 (2019).
 - [40] P. Zeng, W. Wu, and X. Ma, Symmetry-protected privacy: beating the rate-distance linear bound over a noisy channel, Phys. Rev. Applied **13**, 064013 (2020).
 - [41] Y.-M. Xie, B.-H. Li, Y.-S. Lu, X.-Y. Cao, W.-B. Liu, H.-L. Yin, and Z.-B. Chen, Overcoming the rate-distance limit of device-independent quantum key distribution, Opt. Lett. **46**, 1632 (2021).
 - [42] R. Wang, Z.-Q. Yin, F.-Y. Lu, S. Wang, W. Chen, C.-M. Zhang, W. Huang, B.-J. Xu, G.-C. Guo, and Z.-F. Han, Optimized protocol for twin-field quantum key distribution, Commun. Phys. **3**, 149 (2020).
 - [43] B.-H. Li, Y.-M. Xie, Z. Li, C.-X. Weng, C.-L. Li, H.-L. Yin, and Z.-B. Chen, Long-distance twin-field quantum key distribution with entangled sources, Opt. Lett. **46**, 5529 (2021).
 - [44] K. Maeda, T. Sasaki, and M. Koashi, Repeaterless quantum key distribution with efficient finite-key analysis overcoming the rate-distance limit, Nat. Commun. **10**, 3140 (2019).
 - [45] H.-L. Yin and Z.-B. Chen, Finite-key analysis for twin-field quantum key distribution with composable security, Sci. Rep. **9**, 17113 (2019).
 - [46] C. Jiang, Z.-W. Yu, X.-L. Hu, and X.-B. Wang, Unconditional security of sending or not sending twin-field quantum key distribution with finite pulses, Phys. Rev. Ap-

- plied **12**, 024061 (2019).
- [47] G. Currás-Lorenzo, Á. Navarrete, K. Azuma, G. Kato, M. Curty, and M. Razavi, Tight finite-key security for twin-field quantum key distribution, *npj Quantum Inf.* **7**, 22 (2021).
 - [48] M. Minder, M. Pittaluga, G. Roberts, M. Lucamarini, J. Dynes, Z. Yuan, and A. Shields, Experimental quantum key distribution beyond the repeaterless secret key capacity, *Nat. Photonics* **13**, 334 (2019).
 - [49] X. Zhong, J. Hu, M. Curty, L. Qian, and H.-K. Lo, Proof-of-principle experimental demonstration of twin-field type quantum key distribution, *Phys. Rev. Lett.* **123**, 100506 (2019).
 - [50] S. Wang, D.-Y. He, Z.-Q. Yin, F.-Y. Lu, C.-H. Cui, W. Chen, Z. Zhou, G.-C. Guo, and Z.-F. Han, Beating the fundamental rate-distance limit in a proof-of-principle quantum key distribution system, *Phys. Rev. X* **9**, 021046 (2019).
 - [51] Y. Liu, Z.-W. Yu, W. Zhang, J.-Y. Guan, J.-P. Chen, C. Zhang, X.-L. Hu, H. Li, C. Jiang, J. Lin, T.-Y. Chen, L. You, Z. Wang, X.-B. Wang, Q. Zhang, and J.-W. Pan, Experimental twin-field quantum key distribution through sending or not sending, *Phys. Rev. Lett.* **123**, 100505 (2019).
 - [52] X.-T. Fang, P. Zeng, H. Liu, M. Zou, W. Wu, Y.-L. Tang, Y.-J. Sheng, Y. Xiang, W. Zhang, H. Li, Z. Wang, L. You, M.-J. Li, H. Chen, Y.-A. Chen, Q. Zhang, C.-Z. Peng, X. Ma, T.-Y. Chen, and J.-W. Pan, Implementation of quantum key distribution surpassing the linear rate-transmittance bound, *Nat. Photonics* **14**, 422 (2020).
 - [53] J.-P. Chen, C. Zhang, Y. Liu, C. Jiang, W. Zhang, X.-L. Hu, J.-Y. Guan, Z.-W. Yu, H. Xu, J. Lin, M.-J. Li, H. Chen, H. Li, L. You, Z. Wang, X.-B. Wang, Q. Zhang, and J.-W. Pan, Sending-or-not-sending with independent lasers: Secure twin-field quantum key distribution over 509 km, *Phys. Rev. Lett.* **124**, 070501 (2020).
 - [54] H. Liu, C. Jiang, H.-T. Zhu, M. Zou, Z.-W. Yu, X.-L. Hu, H. Xu, S. Ma, Z. Han, J.-P. Chen, Y. Dai, S.-B. Tang, W. Zhang, H. Li, L. You, Z. Wang, Y. Hua, H. Hu, H. Zhang, F. Zhou, Q. Zhang, X.-B. Wang, T.-Y. Chen, and J.-W. Pan, Field test of twin-field quantum key distribution through sending-or-not-sending over 428 km, *Phys. Rev. Lett.* **126**, 250502 (2021).
 - [55] X. Zhong, W. Wang, L. Qian, and H.-K. Lo, Proof-of-principle experimental demonstration of twin-field quantum key distribution over optical channels with asymmetric losses, *npj Quantum Inf.* **7**, 8 (2021).
 - [56] J.-P. Chen, C. Zhang, C. Liu, Yang Jiang, W.-J. Zhang, Z.-Y. Han, S.-Z. Ma, X.-L. Hu, Y.-H. Li, F. Liu, Hui Zhou, H.-F. Jiang, H. Chen, Teng-Yun Li, L.-X. You, Z. Wang, X.-B. Wang, Q. Zhang, and J.-W. Pan, Twin-field quantum key distribution over a 511 km optical fibre linking two distant metropolitan areas, *Nat. Photonics* **15**, 570 (2021).
 - [57] C. Clivati, A. Meda, S. Donadello, S. Virzi, M. Genovese, F. Levi, A. Mura, M. Pittaluga, Z. Yuan, A. J. Shields, M. Lucamarini, I. P. Degiovanni, and D. Calonico, Coherent phase transfer for real-world twin-field quantum key distribution, *Nat. Commun.* **13**, 157 (2022).
 - [58] M. Pittaluga, M. Minder, M. Lucamarini, M. Sanzaro, R. I. Woodward, M.-J. Li, Z. Yuan, and A. J. Shields, 600-km repeater-like quantum communications with dual-band stabilization, *Nat. Photonics* **15**, 530 (2021).
 - [59] J.-P. Chen, C. Zhang, Y. Liu, C. Jiang, D.-F. Zhao, W.-J. Zhang, F.-X. Chen, H. Li, L.-X. You, Z. Wang, Y. Chen, X.-B. Wang, Q. Zhang, and J.-W. Pan, Quantum key distribution over 658 km fiber with distributed vibration sensing, *arXiv preprint arXiv:2110.11671* (2021).
 - [60] S. Wang, Z.-Q. Yin, D.-Y. He, W. Chen, R.-Q. Wang, P. Ye, Y. Zhou, G.-J. Fan-Yuan, F.-X. Wang, W. Chen, Y.-G. Zhu, P. V. Morozov, A. V. Divochiy, Z. Zhou, G.-C. Guo, and Z.-F. Han, Twin-field quantum key distribution over 830-km fibre, *Nat. Photonics* **16**, 154 (2022).
 - [61] L. Kazovsky, Balanced phase-locked loops for optical homodyne receivers: performance analysis, design considerations, and laser linewidth requirements, *J. Light. Technol.* **4**, 182 (1986).
 - [62] L. G. Kazovsky and D. A. Atlas, A 1320-nm experimental optical phase-locked loop: performance investigation and psk homodyne experiments at 140 mb/s and 2 gb/s, *J. Light. Technol.* **8**, 1414 (1990).
 - [63] K. Predehl, G. Grosche, S. M. F. Raupach, S. Droste, O. Terra, J. Alnis, T. Legero, T. W. Hänsch, T. Udem, R. Holzwarth, and H. Schnatz, A 920-kilometer optical fiber link for frequency metrology at the 19th decimal place, *Science* **336**, 441 (2012).
 - [64] A. Huang, A. Navarrete, S.-H. Sun, P. Chaiwongkhot, M. Curty, and V. Makarov, Laser-seeding attack in quantum key distribution, *Phys. Rev. Applied* **12**, 064043 (2019).
 - [65] X.-L. Pang, A.-L. Yang, C.-N. Zhang, J.-P. Dou, H. Li, J. Gao, and X.-M. Jin, Hacking quantum key distribution via injection locking, *Phys. Rev. Applied* **13**, 034008 (2020).
 - [66] M. Lucamarini, I. Choi, M. B. Ward, J. F. Dynes, Z. L. Yuan, and A. J. Shields, Practical security bounds against the trojan-horse attack in quantum key distribution, *Phys. Rev. X* **5**, 031030 (2015).
 - [67] S. Sajeed, A. Huang, S. Sun, F. Xu, V. Makarov, and M. Curty, Insecurity of detector-device-independent quantum key distribution, *Phys. Rev. Lett.* **117**, 250505 (2016).
 - [68] G. Zhang, I. W. Primaatmaja, J. Y. Haw, X. Gong, C. Wang, and C. C. W. Lim, Securing practical quantum communication systems with optical power limiters, *PRX Quantum* **2**, 030304 (2021).
 - [69] M. Bozzio, A. Cavallès, E. Diamanti, A. Kent, and D. Pitalúa-García, Multiphoton and side-channel attacks in mistrustful quantum cryptography, *PRX Quantum* **2**, 030338 (2021).
 - [70] Y. Cao, Y.-H. Li, K.-X. Yang, Y.-F. Jiang, S.-L. Li, X.-L. Hu, M. Abulizi, C.-L. Li, W. Zhang, Q.-C. Sun, W.-Y. Liu, X. Jiang, S.-K. Liao, J.-G. Ren, H. Li, L. You, Z. Wang, J. Yin, C.-Y. Lu, X.-B. Wang, Q. Zhang, C.-Z. Peng, and J.-W. Pan, Long-distance free-space measurement-device-independent quantum key distribution, *Phys. Rev. Lett.* **125**, 260503 (2020).
 - [71] H.-Y. Liu, X.-H. Tian, C. Gu, P. Fan, X. Ni, R. Yang, J.-N. Zhang, M. Hu, J. Guo, X. Cao, X. Hu, G. Zhao, Y.-Q. Lu, Y.-X. Gong, Z. Xie, and S.-N. Zhu, Optical-relayed entanglement distribution using drones as mobile nodes, *Phys. Rev. Lett.* **126**, 020503 (2021).
 - [72] C.-Q. Hu, Z.-Q. Yan, J. Gao, Z.-M. Li, H. Zhou, J.-P. Dou, and X.-M. Jin, Decoy-state quantum key distribution over a long-distance high-loss air-water channel,

- Phys. Rev. Applied **15**, 024060 (2021).
- [73] Y.-A. Chen, Q. Zhang, T.-Y. Chen, W.-Q. Cai, S.-K. Liao, J. K. Chen, J. Yin, J.-G. Ren, Z. Chen, S.-L. Han, Q. Yu, K. Liang, F. Zhou, X. Yuan, M.-S. Zhao, T.-Y. Wang, X. Jiang, L. Zhang, W.-Y. Liu, Y. Li, Q. Shen, Y. Cao, C.-Y. Lu, R. Shu, J.-Y. Wang, L. Li, N.-L. Liu, F. Xu, X.-B. Wang, C.-Z. Peng, and J.-W. Pan, An integrated space-to-ground quantum communication network over 4,600 kilometres, *Nature* **589**, 214 (2021).
 - [74] D. Dequal, L. T. Vidarte, V. R. Rodriguez, G. Vallone, P. Villoresi, A. Leverrier, and E. Diamanti, Feasibility of satellite-to-ground continuous-variable quantum key distribution, *npj Quantum Inf.* **7**, 3 (2021).
 - [75] J. Yin, Y.-H. Li, S.-K. Liao, M. Yang, Y. Cao, L. Zhang, J.-G. Ren, W.-Q. Cai, W.-Y. Liu, S.-L. Li, *et al.*, Entanglement-based secure quantum cryptography over 1,120 kilometres, *Nature* **582**, 501 (2020).
 - [76] H. Takenaka, A. Carrasco-Casado, M. Fujiwara, M. Kitamura, M. Sasaki, and M. Toyoshima, Satellite-to-ground quantum-limited communication using a 50-kg-class microsatellite, *Nat. Photonics* **11**, 502 (2017).
 - [77] S. Wehner, D. Elkouss, and R. Hanson, Quantum internet: A vision for the road ahead, *Science* **362**, eaam9288 (2018).
 - [78] J. S. Sidhu, S. K. Joshi, M. Gündoğan, T. Brougham, D. Lowndes, L. Mazzarella, M. Krutzik, S. Mohapatra, D. Dequal, G. Vallone, P. Villoresi, A. Ling, T. Jennewein, M. Mohageg, J. G. Rarity, I. Fuentes, S. Pirandola, and D. K. L. Oi, Advances in space quantum communications, *IET Quantum Commun.* **2**, 182 (2021).
 - [79] X. Ma and M. Razavi, Alternative schemes for measurement-device-independent quantum key distribution, *Phys. Rev. A* **86**, 062319 (2012).
 - [80] Y.-M. Xie, C.-X. Weng, Y.-S. Lu, Y. Fu, Y. Wang, H.-L. Yin, and Z.-B. Chen, Scalable high-rate twin-field quantum key distribution networks without constraint of probability and intensity, *arXiv preprint arXiv:2112.11165* (2021).
 - [81] H. Xu, Z.-W. Yu, C. Jiang, X.-L. Hu, and X.-B. Wang, Sending-or-not-sending twin-field quantum key distribution: Breaking the direct transmission key rate, *Phys. Rev. A* **101**, 042330 (2020).
 - [82] C. Jiang, X.-L. Hu, H. Xu, Z.-W. Yu, and X.-B. Wang, Zigzag approach to higher key rate of sending-or-not-sending twin field quantum key distribution with finite-key effects, *New J. Phys.* **22**, 053048 (2020).
 - [83] K. Azuma, K. Tamaki, and W. J. Munro, All-photonics intercity quantum key distribution, *Nat. Commun.* **6**, 10171 (2015).
 - [84] S. Bose and D. Home, Duality in entanglement enabling a test of quantum indistinguishability unaffected by interactions, *Phys. Rev. Lett.* **110**, 140404 (2013).
 - [85] H.-K. Lo, X. Ma, and K. Chen, Decoy state quantum key distribution, *Phys. Rev. Lett.* **94**, 230504 (2005).
 - [86] X.-B. Wang, Beating the photon-number-splitting attack in practical quantum cryptography, *Phys. Rev. Lett.* **94**, 230503 (2005).
 - [87] H. Takesue, S. W. Nam, Q. Zhang, R. H. Hadfield, T. Honjo, K. Tamaki, and Y. Yamamoto, Quantum key distribution over a 40-dB channel loss using superconducting single-photon detectors, *Nat. Photonics* **1**, 343 (2007).
 - [88] N. T. Islam, C. C. W. Lim, C. Cahall, J. Kim, and D. J. Gauthier, Provably secure and high-rate quantum key distribution with time-bin qudits, *Sci. Adv.* **3**, e1701491 (2017).
 - [89] H. Chernoff, A measure of asymptotic efficiency for tests of a hypothesis based on the sum of observations, *Ann. Math. Stat.* **23**, 493 (1952).
 - [90] H.-L. Yin, M.-G. Zhou, J. Gu, Y.-M. Xie, Y.-S. Lu, and Z.-B. Chen, Tight security bounds for decoy-state quantum key distribution, *Sci. Rep.* **10**, 14312 (2020).
 - [91] H.-K. Lo and J. Preskill, Security of quantum key distribution using weak coherent states with nonrandom phases, *Quantum Inf. Comput.* **7**, 431 (2007).
 - [92] M. Koashi, Simple security proof of quantum key distribution based on complementarity, *New J. Phys.* **11**, 045018 (2009).
 - [93] H.-K. Lo, Proof of unconditional security of six-state quantum key distribution scheme, *Quantum Inf. Comput.* **1**, 81 (2001).
 - [94] H.-L. Yin, Y. Fu, Y. Mao, and Z.-B. Chen, Security of quantum key distribution with multiphoton components, *Sci. Rep.* **6**, 29482 (2016).
 - [95] P. Zeng, H. Zhou, W. Wu, and X. Ma, Quantum key distribution surpassing the repeaterless rate-transmittance bound without global phase locking, *arXiv preprint arXiv:2201.04300* (2022).